AD-A120 949 ON THE USE OF BOREHOLES IN CONTROLLED ELECTROMAGNETIC SOURCE SOUNDINGS OF..(U) SCRIPPS INSTITUTION OF OCEANOGRAPHY LA JOLLA CA A D CHAVE ET AL. SEP 82 1/1

UNCLASSIFIED SIO-REF-82-24 N00014-75-C-0999 F/G 8/7 NL

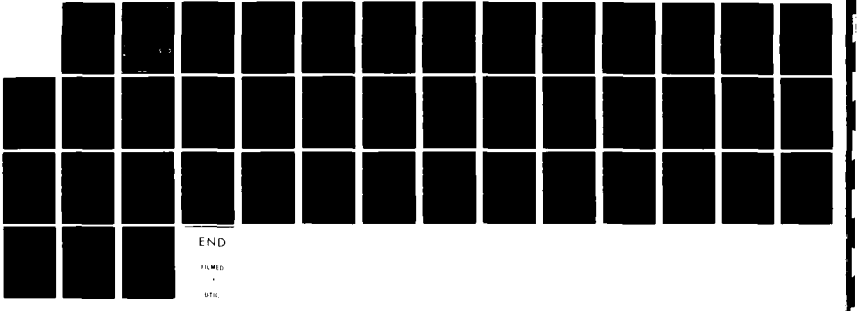

END

FILMED

DTIC

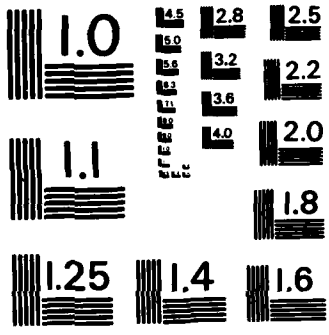

MICROCOPY RESOLUTION TEST CHART
NATIONAL BUREAU OF STANDARDS - 1963 - A

(12)

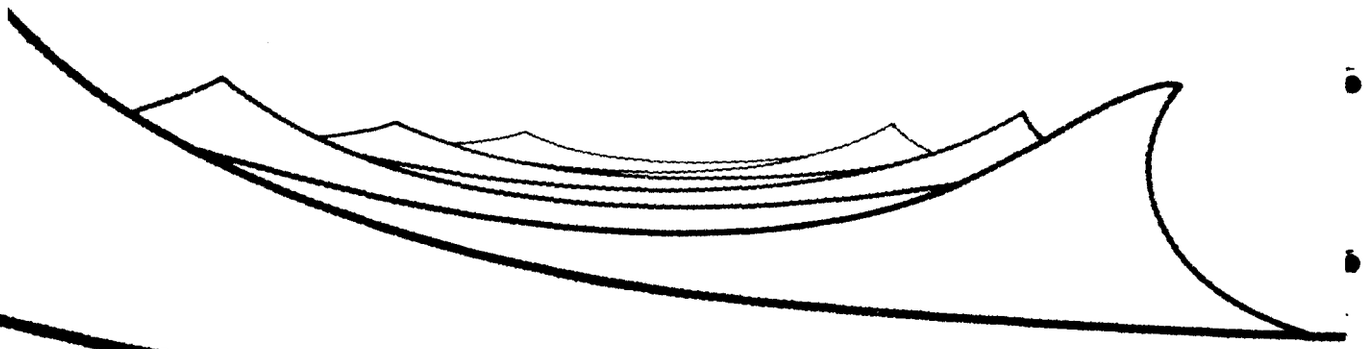

SIO REFERENCE SERIES

On the Use of Boreholes in Controlled Electromagnetic Source Soundings of the Ocean Crust

Alan D. Chave
and
Charles S. Cox

SIO Reference 82-24

University of California Scripps Institution of Oceanography

Unclassified

SECURITY CLASSIFICATION OF THIS PAGE *(When Data Entered)*

REPORT DOCUMENTATION PAGE		READ INSTRUCTIONS BEFORE COMPLETING FORM
1. REPORT NUMBER SIO Ref. 82-24	2. GOVT ACCESSION NO. AD-A120 949	3. RECIPIENT'S CATALOG NUMBER
4. TITLE *(and Subtitle)* ON THE USE OF BOREHOLES IN CONTROLLED ELECTROMAGNETIC SOURCE SOUNDINGS OF THE OCEAN CRUST		5. TYPE OF REPORT & PERIOD COVERED 6. PERFORMING ORG. REPORT NUMBER SIO Ref. 82-24
7. AUTHOR(s) Alan D. chave and Charles S. Cox		8. CONTRACT OR GRANT NUMBER(s) N00014-75-C-0999
9. PERFORMING ORGANIZATION NAME AND ADDRESS Scripps Institution of Oceanography La Jolla, CA 92093		10. PROGRAM ELEMENT, PROJECT, TASK AREA & WORK UNIT NUMBERS
11. CONTROLLING OFFICE NAME AND ADDRESS Office of Naval Research Arlington, VA 22217		12. REPORT DATE September 1982 13. NUMBER OF PAGES 39
14. MONITORING AGENCY NAME & ADDRESS*(if different from Controlling Office)*		15. SECURITY CLASS. *(of this report)* Unclassified 15a. DECLASSIFICATION/DOWNGRADING SCHEDULE

16. DISTRIBUTION STATEMENT *(of this Report)*

Approved for public release: Distribution unlimited.

17. DISTRIBUTION STATEMENT *(of the abstract entered in Block 20, if different from Report)*

18. SUPPLEMENTARY NOTES

19. KEY WORDS *(Continue on reverse side if necessary and identify by block number)*

20. ABSTRACT *(Continue on reverse side if necessary and identify by block number)*

Natural electromagnetic fields at the floor of the deep ocean have been used to infer the electrical conductivity of the upper mantle using the passive magnetotelluric method (Cox et al. 1970, Filloux 1980, Chave et al. 1981). All such studies indicate rising electrical conductivity at depths of 50-100 km, but the data cannot resolve either the conductivity or the thickness of the crust or upper lithosphere where the electrical conductivity may be lower. This is due in large part to the band limited...

DD FORM 1 JAN 73 1473 EDITION OF 1 NOV 65 IS OBSOLETE

S/N 0102-LF-014-6601

SECURITY CLASSIFICATION OF THIS PAGE *(When Data Entered)*

Scripps Institution of Oceanography
University of California at San Diego

On the Use of Boreholes in Controlled Electromagnetic Source Sounding of the Ocean Crust

Alan D. Chave

and

Charles S. Cox

Scripps Institution of Oceanography

La Jolla, CA 92093

Prepared for the Office of Naval Research under

Contract N00014-75-C-0999

September 1982

SIO Reference 82-24

1. Introduction

Natural electromagnetic fields at the floor of the deep ocean have been used to infer the electrical conductivity of the upper mantle using the passive magnetotelluric method (Cox *et al.* 1970, Filloux 1980, Chave *et al.* 1981). All such studies indicate rising electrical conductivity at depths of 50-100 km, but the data cannot resolve either the conductivity or the thickness of the crust or upper lithosphere where the electrical conductivity may be lower. This is due in large part to the band limited nature of the seafloor electromagnetic spectrum and the probable presence of ocean-generated source fields of variable but unknown spatial morphology. In any case, the modal structure of the electromagnetic field induced by external sources is the poloidal magnetic type in the terminology of Chave (1982) and is quite insensitive to low conductivity material.

The existence of low conductivity regions in the upper lithosphere is suggested by laboratory data on various minerals. Such a region would exert a profound influence on the interpretation of both motional induction fields caused by large scale oceanic flows and magnetotelluric experiments in the ocean-continent transition region (Cox 1980, 1981). If the conductivity of any possible lithospheric channel were low enough and its horizontal extent were basin-wide, then potential military applications for secure, electromagnetic pulse-proof communications would arise.

The background magnetic spectral density in the frequency band centered near 1 Hz is about $10^{-23}(V/m)^2/Hz$ at the floor of the deep ocean (Cox *et al.* 1978). This is at least one million times lower than is observed on land due to the shielding effect of the ocean and the absence of any significant seafloor noise sources. This led Cox (1980) to propose the use of seafloor-

based controlled electromagnetic sources using frequencies within two decades of 1 Hz to probe the conductivity of the oceanic crust and lithosphere. Two approaches using vertical (Edwards et al 1981) and horizontal (Young and Cox 1981, Chave and Cox 1982) electric dipole (VED and HED) sources have been proposed or applied to date.

In this report the theory of Chave and Cox (1982) is extended to the case where either the source or receiver is located in the oceanic crust, as in a borehole. Numerical calculations are presented which indicate that very little is gained by the use of boreholes unless low conductivity (< 0.005 S/m) material is penetrated for a significant distance, an unlikely occurrence unless the hole is deeper than 1500-2000 m. In particular, a VED source located in a borehole with receivers placed on the seafloor yields generally weaker signals than HED sources and receivers both located on the seafloor. A seafloor-based HED source with borehole receiver shows greater promise in terms of signal strength, however engineering limitations for this arrangement are more severe.

2. Theory

The relevant theory is an extension of that presented by Chave and Cox (1982). The Maxwell equations of electromagnetism may be written in the form

$$\bar{\nabla} \cdot \bar{B} = 0 \tag{1}$$

$$\bar{\nabla} \times \bar{B} = \mu\sigma\bar{E} + \mu\bar{J}^0 \tag{2}$$

$$\bar{\nabla} \times \bar{E} = -\partial_t \bar{B} \tag{3}$$

where $\bar{B}$ is the magnetic induction, $\bar{E}$ is the induced electric field, $\bar{J}^0$ is the specified or impressed source electric current, μ is the magnetic permeability, usually taken as the free space value μ_0, and σ is the electrical

conductivity. If the electrical structure of the earth is assumed to be one dimensional, then (1) - (3) can be rewritten in terms of two scalar functions Π and Ψ (Chave 1982)

$$\bar{B} = \bar{\nabla} \times (\Pi\hat{z}) + \bar{\nabla} \times \bar{\nabla} \times (\Psi\hat{z}) \tag{4}$$

$$\bar{E} = \bar{\nabla}\left|\partial_z \Pi/\mu\sigma - T/\sigma\right| - \partial_t \Pi\hat{z} - \bar{\nabla} \times (\partial_t \Psi\hat{z}) \tag{5}$$

where

$$\bar{J}^0 = J_z^0\hat{z} + \bar{\nabla}_h T + \bar{\nabla} \times (Y\hat{z}) \tag{6}$$

and the governing differential equations are

$$\bar{\nabla}_h^2 \Pi + \mu\sigma\partial_z(\partial_z \Pi/\mu\sigma) - \mu\sigma\partial_t \Pi = -\mu J_z^0 + \mu\sigma\partial_z(T/\sigma) \tag{7}$$

$$\bar{\nabla}^2 \Psi - \mu\sigma\partial_t \Psi = -\mu Y \tag{8}$$

The source current terms in (6) are the solutions of the Poisson equations

$$\bar{\nabla}_h^2 T = \bar{\nabla}_h \cdot \bar{J}^0 \tag{9}$$

$$\bar{\nabla}_h^2 Y = -(\bar{\nabla} \times \bar{J}^0) \cdot \hat{z} \tag{10}$$

The separation of (4) - (10) is far more than a mathematical convenience. The scalar terms Π and Ψ represent the two independent modes of induced current flow in a one-dimensional earth. The Ψ function represents the transverse electric (TE) or poloidal magnetic mode where electric current flows parallel to the earth's surface everywhere, with coupling to deep structure occurring by induction. The Π function represents the transverse magnetic (TM) or toroidal magnetic mode, where the induced electric current flows in loops containing the vertical direction. TE modes are analogous to the magnetotelluric situation, and are quite insensitive to low conductivity regions since they can couple across them by mutual induction. TM modes are analogous to DC currents, and are by contrast very sensitive to low conductivity zones since vertical electric currents cannot penetrate them.

For artificial source work there are four fundamental source types: the vertical and horizontal electric dipoles (VED and HED) and the vertical and horizontal magnetic dipole (VMD and HMD). The VED and HMD can induce only TM modes, the VMD can induce only TE modes, while the HED produces a combination of the two. Chave and Cox (1982) showed that the HED produces the best coupling between ocean and earth, while Edwards et al. (1981) considered the DC limit and a VED source. The VMD and HMD sources are not practical in the ocean for engineering reasons, except possibly on a very small scale. In succeeding sections, a VED source located in the ocean crust with seafloor receivers and an HED source on the seafloor with borehole receivers will be considered in detail.

2.1 VED Borehole Source

The ocean is assumed to occupy the region $0 \leq z \leq H$ with conductivity σ_0, air is the region $z > H$, while the VED source stretches from $z = -L$ to $z = 0$ with crustal conductivity σ_1, and an arbitrary conductivity structure is located below $z = -L$. The electromagnetic fields must satisfy (7) since only TM modes need be considered, yielding

$$\vec{\nabla}\Pi - i\omega\mu_0\sigma\Pi = -\mu J_z^0 \tag{11}$$

where the right hand side vanishes outside $-L \leq z \leq 0$ and $e^{i\omega t}$ sinusoidal time dependence is assumed. The appropriate solution of (4) - (6) and (11) is most easily obtained by rewriting the Green functions obtained by Chave (1982) in the form

$$\hat{\Pi} = -\frac{e^{-\beta_1|z-z'|} + R_L e^{-2\beta_1 L} e^{-\beta_1(z+z')} + R_U e^{\beta_1(z+z')} + R_U R_L e^{-2\beta_1 L} e^{\beta_1|z-z'|}}{2\beta_1(1-R_U R_L e^{-2\beta_1 L})} \tag{12}$$

where z and z' are the observation and source heights,

$$\beta_i = \sqrt{k^2 + i\omega\mu_0\sigma_i} \tag{13}$$

in the region of conductivity σ_i with horizontal wavenumber k, and the spatial dependence is recovered from the Bessel transform

$$\Pi = \int_0^\infty dk J_0(k\rho)\hat{k\Pi} \tag{14}$$

where J_0 is the Bessel function of the first kind of order 0 and ρ is the horizontal range. R_U and R_L are the reflection coefficients at the z = 0 and z = -L interfaces respectively, given by

$$R_U = \frac{\alpha\tanh\beta_0 H - 1}{\alpha\tanh\beta_0 H + 1}$$

$$R_L = \frac{\frac{\beta_1}{\sigma_1}K - 1}{\frac{\beta_1}{\sigma_1}K + 1} \tag{15}$$

where $\alpha = \beta_1\sigma_0/\beta_0\sigma_1$ and K is the TM mode response function described by Chave and Cox (1982) and Chave (1982) which contains all of the necessary information about the conductivity below z = L. For a finite VED extending from z = -L to z = 0 the Green function (12) is integrated to yield

$$\hat{\Pi} = \frac{\mu_0 I}{4\pi}\left[\frac{2}{\beta_1^2} + \frac{(R_U - 1)(e^{\beta_1 z} + R_L e^{-2\beta_1 L} e^{-\beta_1 z}) + (R_L - 1)(e^{-\beta_1(L+z)} + R_U e^{-\beta_1(L-z)})}{\beta_1^2(1 - R_U R_L e^{-2\beta_1 L})}\right] \tag{16}$$

where I is the source current. This expression holds only in the source region ($-L \leq z \leq 0$), and the solution in the ocean is of the form

$$\hat{\Pi} = Ae^{-\beta_0 z} + Be^{\beta_0 z} \tag{17}$$

where A and B are obtained by matching the boundary conditions at z = 0 (continuity of Π and $\partial_z\Pi/\sigma$).

After some tedious algebra, the results are

$$A = \left[\frac{1}{\beta_1^2} + \frac{\sigma_0}{2\beta_0}\left[\frac{\Gamma - \Delta}{\beta_1^2(1 - R_U R_L e^{-2\beta_1 L})}\right]\right] \tag{18}$$

$$B = \left[\frac{1}{\beta_1^2} + \frac{\sigma_0}{2\beta_0}\left[\frac{\Gamma + \Delta}{\beta_1^2(1 - R_U R_L e^{-2\beta_1 L})}\right]\right] \tag{19}$$

where

$$\Gamma = \frac{\beta_0}{\sigma_0}\left[(R_U - 1)(1 + R_L e^{-2\beta_1 L}) + (R_L - 1)(R_U + 1)e^{-\beta_1 L}\right]$$

$$\Delta = \frac{\beta_1}{\sigma_1}\left[(R_U - 1)(1 - R_L e^{-2\beta_1 L}) + (R_L - 1)(R_U - 1)e^{-\beta_1 L}\right]$$

By symmetry, only three nonzero electromagnetic field components are obtained from (4) and (5)

$$E_\rho = \frac{I}{4\pi\sigma_0}\int_0^\infty dk J_1(k\rho)k^2\beta_0\left[Ce^{-\beta_0 z} - De^{\beta_0 z}\right] \tag{20}$$

$$E_z = \frac{I}{4\pi\sigma_{00}}\int_0^\infty dk J_0(k\rho)k^3\left[Ce^{-\beta_0 z} + De^{\beta_0 z}\right] \tag{21}$$

$$B_\phi = \frac{\mu_0 I}{4\pi}\int_0^\infty dk J_1(k\rho)k^2\left[Ce^{-\beta_0 z} + De^{\beta_0 z}\right] \tag{22}$$

where $C = \frac{\mu_0 I}{4\pi}A$ and $D = \frac{\mu_0 I}{4\pi}B$.

2.2. Borehole Measurement of a Seafloor HED Source

The mathematical development for this case is also very similar to the seafloor source-receiver case treated in detail by Chave and Cox (1982). The solutions for a borehole occupying $-L \leq z \leq 0$ are given by

$$\Psi = -\frac{\mu_0 p}{4\pi}\partial_y\int_0^\infty dk J_0(k\rho)T_U^{TE}e^{-\beta_0 z'}\frac{e^{\beta_1 z} + R_L^{TE}e^{-\beta_1 z}e^{-2\beta_1 L}}{1 - R_U^{TE}R_L^{TE}e^{-2\beta_1 L}} \tag{23}$$

$$\Pi = \frac{\mu_0 p}{4\pi}\partial_{x_0}\int_0^\infty dk J_0(k\rho) T_U^{TM} e^{-\beta_0 z'} \frac{e^{\beta_1 z} + R_L^{TM} e^{-\beta_1 z} e^{-2\beta_1 L}}{1 - R_U^{TM} R_L^{TM} e^{-2\beta_1 L}} - \tag{24}$$

for an infinitesimal source at $0 \leq z' \leq \infty$ with a strength p. The extension to a finite source is detailed in Appendix A of Chave and Cox (1982). T_U^{TE} and T_U^{TM} are seafloor transmission coefficients given by

$$T_U^{TE} = \frac{2\beta_0}{\beta_0 + \beta_1} \tag{25}$$

$$T_U^{TM} = \frac{2\frac{\beta_0}{\sigma_0}}{\frac{\beta_0}{\sigma_0} + \frac{\beta_1}{\sigma_1}}$$

while R_U^{TE} and R_U^{TM} are the seafloor reflection coefficients

$$R_U^{TE} = \frac{\beta_1 - \beta_0}{\beta_1 + \beta_0} \tag{26}$$

$$R_U^{TM} = \frac{\frac{\beta_1}{\sigma_1} - \frac{\beta_0}{\sigma_0}}{\frac{\beta_1}{\sigma_1} + \frac{\beta_0}{\sigma_0}}$$

and R_L^{TE} and R_L^{TM} are the $z = -L$ reflection coefficients

$$R_L^{TE} = \frac{\beta_1 \Lambda - 1}{\beta_1 \Lambda + 1} \tag{27}$$

$$R_L^{TM} = \frac{\frac{\beta_1}{\sigma_1} K - 1}{\frac{\beta_1}{\sigma_1} K + 1}$$

with the response functions Λ and K given in Chave and Cox (1982). The six electromagnetic field components follow from (4) and (5). Defining the four

terms

$$A(k) = \frac{e^{\beta_1 z} + R_L^{TE} e^{-\beta_1 z} e^{-2\beta_1 L}}{1 - R_U^{TE} R_L^{TE} e^{-2\beta_1 L}} e^{-\beta_0 z'} \tag{28}$$

$$B(k) = -\frac{e^{\beta_1 z} - R_L^{TE} e^{-\beta_1 z} e^{-2\beta_1 L}}{1 - R_U^{TE} R_L^{TE} e^{-2\beta_1 L}} e^{-\beta_0 z'} \tag{29}$$

$$C(k) = \frac{e^{\beta_1 z} + R_L^{TM} e^{-\beta_1 z} e^{-2\beta_1 L}}{1 - R_U^{TM} R_L^{TM} e^{-2\beta_1 L}} e^{-\beta_0 z'} \tag{30}$$

$$D(k) = -\frac{e^{\beta_1 z} - R_L^{TM} e^{-\beta_1 z} e^{-2\beta_1 L}}{1 - R_U^{TM} R_L^{TM} e^{-2\beta_1 L}} e^{-\beta_0 z'} \tag{31}$$

yields

$$E_\rho = a \cos \phi \left[\int_0^\infty dk I(k\rho) T_U^{TM} \beta_1 D(k) - \frac{1}{\rho_0} \int_0^\infty dk J_1(k\rho) T_U^{TE} \frac{\gamma_1^2}{\beta_0} A(k) \right] \tag{32}$$

$$E_\phi = a \sin \phi \left[\int_0^\infty dk I(k\rho) T_U^{TE} \frac{\gamma_1^2}{\beta_0} A(k) - \frac{1}{\rho_0} \int_0^\infty dk J_1(k\rho) T_U^{TM} \beta_1 D(k) \right] \tag{33}$$

$$E_z = -a \cos \phi \int_0^\infty dk J_1(k\rho) T_U^{TM} k^2 C(k) \tag{34}$$

$$B_\rho = b \sin \phi \left[\int_0^\infty dk I(k\rho) T_U^{TE} \frac{\beta_1}{\beta_0} B(k) - \frac{1}{\rho} dk J_1(k\rho) T_U^{TM} C(k) \right] \tag{35}$$

$$B_\phi = b \cos \phi \left[\int_0^\infty dk I(k\rho) T_U^{TM} C(k) - \frac{1}{\rho_0} \int_0^\infty dk J_1(k\rho) T_U^{TE} \frac{\beta_1}{\beta_0} B(k) \right] \tag{36}$$

$$B_z = b \sin \phi \int_0^\infty dk J_1(k\rho) T_U^{TE} \frac{k^2}{\beta_0} A(k) \tag{37}$$

where $a = p/4\pi\sigma_1$, $b = \mu_0 p/4\pi$, ϕ is the azimuthal angle measured with respect to the source wire, and $I(k\rho) = kJ_0(k\rho) - J_1(k\rho)/\rho$.

2.3. Numerical Methods

The field expressions (20)-(22) and (32)-(37) were evaluated using Gauss quadrature between the asymptotic zero crossings of the Bessel fnctions J_0 and J_1 with Pade summation of the resulting series of partial integrations. For details, see Chave and Cox (1982).

3. Model Studies

In this section, the electromagnetic response of a series of models of the upper lithosphere will be examined. Similar examples to those used by Chave and Cox (1982) will be used when possible to facilitate comparison of borehole methods with the seafloor approach. Some additional models containing a deep, low conductivity channel, as postulated for the continental lithosphere by Simmons et al. (1980), will also be explored.

Figure 1 shows the radial and vertical electric and magnetic fields for a seafloor HED source and receiver as a function of range at a frequency of 1 Hz. The ocean model has a conductivity of 3.2 S/m and the underlying lithospheric halfspace has a conductivity of 0.05 S/m; the corresponding e-folding or skin depths are 270 m in the ocean and 2.25 km in rock. Note that the infinitesimal source has a strength of 1 A-m, a factor of 10^4 - 10^5 smaller than can be used in practical experiments. Attenuation of the electromagnetic fields in a quasi-exponential fashion with range is apparent, while the phase decays at about one radian per skin depth in the lithosphere. The direct field propagating in the highly conductive ocean decays very rapidly with range, and the observed fields at ranges over a few km are those traveling in the lower conductivity rock. The horizontal components of both the electric and magnetic fields are at least ten times larger than their corresponding vertical components at all ranges.

Figure 2 shows the corresponding results for a borehole VED source and seafloor-based receivers. The source occupies the upper 500 m of the lower halfspace. As for the seafloor-to-seafloor case, the horizontal electric field exceeds the vertical component by about a factor of ten. The horizontal electric and magnetic field amplitudes in Figures 1 and 2 are comparable, while the vertical electric field is significantly stronger at range, reflecting the slower decay rate of the VED field (21), when compared to the HED results in Chave and Cox (1982). Note that the assumed length of the source is dictated by practical considerations and that the field components (20)-(22) are dependent on this length.

Figure 3 shows the results obtained by borehole measurement of a seafloor-based HED source. By contrast to the seafloor-to-seafloor and VED cases, the vertical electric field is larger than the horizontal component near the source, and the vertical magnetic field is comparable to its horizontal counterpart. The borehole vertical electric field is smaller than the horizontal component of Figure 1 at all ranges, and the horizontal magnetic components are more nearly equal in Figures 1 and 3. Note that the reciprocity theorem of electromagnetism requires that the seafloor horizontal electric fields produced by a borehole VED source and the borehole vertical electric field produced by a seafloor HED source be equivalent; this is seen in Figures 2 and 3.

The differences observed between Figures 1-3 can be understood in a qualitative fashion by a simple application of the law of refraction. For a horizontal source in a highly conducting region like the ocean, the electric fields are largely horizontal, while the refracted lines in the lower conductivity rock will be nearly vertical. Similar arguments show that a borehole

VED will produce largely horizontal fields in the ocean. This qualitative argument cannot be used to assess the relative utility of the three cases treated since the actual field magnitudes depend critically on the electrical conductivity structure below the source.

Chave and Cox (1982) presented a model for the electrical conductivity of the ocean crust based on ophiolite and laboratory data. The seafloor-to-seafloor electromagnetic response for one possible model, consisting of a 1 km pillow basalt layer of conductivity 0.05 S/m, a 2.5 km gabbro layer of conductivity 0.003 S/m, and a 2 km sheeted dike region of conductivity 0.001 S/m overlying a 0.0005 S/m halfspace, is reproduced as Figure 4. The corresponding result for a borehole VED in the top 500 m of the pillow layer is shown in Figure 5. The horizontal electric field amplitude is in all instances lower for the borehole VED source at long range and comparable at a few km range. The relative changes in both amplitude and phase produced by the crustal conductivity structure is smaller for the VED source, suggesting decreased resolving power. In particular, the very large phase changes of Figure 4 are not seen in Figure 5.

Figure 6 displays results corresponding to Figure 4 for the azimuthal magnetic field for a seafloor HED to seafloor receiver and the same crustal model. Very similar behavior to the electric field result of Figure 4 is seen. Figure 7 shows the same field component from the same source at a depth of 500 m in a borehole in the upper layer of the crust. The magnetic field amplitudes are similar for the two cases, but the relative changes produced by the crustal structure are very much smaller for the borehole receiver. The large amplitude change at low frequencies for the seafloor-to-seafloor path are caused by the geophysically uninteresting direct wave in the water.

Figure 8 shows three models of the upper lithosphere containing a subcrustal low conductivity channel. In all cases the ocean is a halfspace of conductivity 3.2 S/m, while the crustal model of Figure 4 is simplified to a 5.5 km layer of conductivity 0.003 S/m. This neglects the high conductivity pillow basalt layer and will produce an optimistic estimate of the field amplitudes. Models 1 and 2 have a 4 km region of conductivity 0.0002 S/m underlying the crust, and a 10 km thick low conductivity channel at 10^{-6} S/m for Model 1 and 10^{-5} S/m for Model 2. Model 3 differs from Model 2 in the subcrustal layer, which has a much lower conductivity of 5×10^{-5} S/m. This value is possible only if mantle rocks contain essentially no free water.

Figures 9-11 compare the amplitude of the horizontal electric field produced by the seafloor HED to seafloor receiver with the borehole VED source to seafloor receiver and seafloor HED source to borehole receiver for these earth models. In each case, an upper 500 m crustal conductivity of 0.05 S/m or 0.005 S/m is used for the borehole cases; the former is consistent with measurements from DSDP holes in the upper 1 km of the crust (von Herzen et al. 1982), while the latter is consistent with much deeper crustal structure. For Models 1 and 2 the VED source produces weaker fields than the seafloor HED, while this situation reverses for the lower subcrustal conductivity case of Model 3. The borehole receiver and seafloor HED consistently produces slightly higher field amplitudes, especially for the low conductivity crust, but the differences are less than a factor of ten. The phases (not shown) are consistent with the results of Figure 4-7, with smaller changes occurring when the borehole is used.

4. Discussion

The preceding models indicate only the expected signal levels and relative changes caused by conductive structure. The separate question of resolution, or the ability to quantitatively estimate conductive structure from field measurements, was not addressed. The fact that both borehole techniques produce markedly lower relative changes in the electromagnetic fields when compared to the seafloor method suggests that, for a given signal-to-noise ratio, the seafloor technique will yield better results.

The estimation of various experimental parameters, notably antenna resistances and required source voltage and current, are discussed by Cox et al. (1980) for the seafloor HED technique. Some simple calculations will allow their extension to borehole methods. For the borehole VED, the transmitting antenna is located in a medium of resistivity ρ, has an electrode length $2L$, and a radius a, and approximating its shape by a prolate spheroid yields a resistance to infinity of

$$R = \frac{\rho}{8\pi\sqrt{L^2 - a^2}} \log \left[\frac{L + \sqrt{L^2 - a^2}}{L - \sqrt{L^2 - a^2}} \right] \tag{38}$$

This can be approximated, when $a/L \ll 1$, as

$$R = \frac{\rho}{4\pi L} \log \left[\frac{2L}{a} \right] \tag{39}$$

For practical purposes, L may be of order 25 m, while a is the radius of the borehole (10 - 20 cm). For the upper oceanic crust, the rock resistivity is 20 Ω - m, increasing to 200 Ω - m deeper down. This yields an antenna resistance of 0.4 to 4 Ω, a value which must be doubled to include both electrodes, and the intrinsic resistance of the antenna wire (typically 1Ω) must be added to yield a total resistance of 2 - 10 Ω. To get a source moment of 10^5 A-m,

similar to the seafloor HED, will require a source current of 200 A for a 500 m long antenna. This in turn requires a generator capable of delivering $P = I^2R$ watts, yielding P = 80 - 400 kw. Such large capacities are rarely available, and a reduced antenna current, and concomitant reduction in source moment, will undoubtedly result. It should be noted that this is a pessimistic estimate since L was taken only as the length of the bared wire end of the antenna, and its effective length will be larger due to the presence of conductive seawater in the borehole. This is not likely to change the results by more than a factor of 2-4, and it would require a factor of over 20 to make the deep crustal source practical. Since it is only a deep crustal VED, located in material of conductivity below .05 S/m, which yields any advantages over the seafloor HED, this suggests that the borehole VED source is not favored. The seafloor HED to borehole receiver may be somewhat more practical if deep penetration, into the lower crust, is obtained. Clearly reception of the horizontal electric field is impractical in a confined hole, and the vertical electric field strength is not large at long source receiver ranges from Fig. 3. The use of magnetometers may yield better results, especially if SQUID types or the collector-type fluxgate can be adapted. The motion problem, which is a serious limitation on the seafloor, may be smaller in a borehole. This requires further study. In any case, only deep (> 2 km) boreholes in the ocean crust will yield any real advantage over the seafloor-to-seafloor method, and such holes are hideously expensive to drill. For example, DSDP Hole 504B, which penetrated to 1400. m in the ocean crust on the Costa Rica Rift, required three drilling legs of 1 1/2 - 2 mos. each on Glomar Challenger.

References

Chave, A.D. 1982. On the theory of EM induction in the earth by ocean currents. J. Geophys. Res. Submitted.

Chave, A.D., R.P. von Herzen, K.A. Poehls and C.S. Cox 1981. EM induction fields in the deep ocean northeast of Hawaii: implications for mantle conductivity and source fields. Geophys. J. Roy. Astr. Soc. 66, 379-406.

Chave, A.D. and C.S. Cox 1982. Controlled EM sources for measuring electrical conductivity beneath the oceans, 1, forward problem and model study. J. Geophys. Res. 87, 5327-5338.

Cox, C.S. 1980. EM induction in the oceans and inferences on the constitution of the earth. Geophys. Surv. 4, 137-156.

Cox, C.S. 1981. On the electrical conductivity of the oceanic lithosphere. Phys. Earth Pl. Int. 25, 196-201.

Cox, C.S., J.H. Filloux and J.C. Larsen 1970. EM studies of ocean currents and electrical conductivity below the ocean floor, in A.E. Maxwell (ed), The Sea, Vol. 4 Pt. 1, pp. 637-693.

Cox, C.S., N. Kroll, P. Pistek and K. Watson 1978. EM fluctuations induced by wind waves on the deep-sea floor. J. Geophys. Res. 83, 431-442.

Cox, C.S., T. Deaton and P. Pistek 1980. An active source EM method for the seafloor. Radio Sci. Submitted.

Edwards, R.N., L.K. Law and J.M. DeLaurier 1981. On measuring the electrical conductivity of the ocean crust by a modified magnetometric resistivity method. J. Geophys. Res. 86, 11607-11615.

Filloux, J.H. 1981. Magnetotelluric exploration of the North Pacific: progress report and preliminary soundings near a spreading ridge. Phys. Earth Pl. Int. 25, 187-195.

Simmons, G., L. Caruso and F. Miller 1980. The electrical conductivity of the crust of the eastern United States. Technical report, MIT. (Unpublished manuscript.)

von Herzen, R.P., T.J.G. Francis and K. Becker 1982. In-situ large scale electrical resistivity of ocean crust, site 504B. Initial Rept. Deep Sea Drilling Proj. 69/70. In press.

Young, P.D. and C.S. Cox 1981. EM active source sounding near the East Pacific Rise. Geophys. Res. Lett. 8, 1043-1046.

Figure 1

The electric and magnetic fields produced at the seafloor by a seafloor-based HED source as a function of range for a source frequency of 1 Hz. The radial (solid line) and vertical (dashed line) components are shown for the electric field (left panels) at an azimuth of 0^{o} and the magnetic field (right panels) at an azimuth of 90^{o}. Azimuth is the angle measured with respect to the end of the source. The ocean conductivity is taken as 3.2 S/m, while the rock halfspace has a conductivity of 0.05 S/m. The source dipole is infinitesimal in extent with a source moment of 1 A-m. (Taken from Chave and Cox, 1982, Figure 4.)

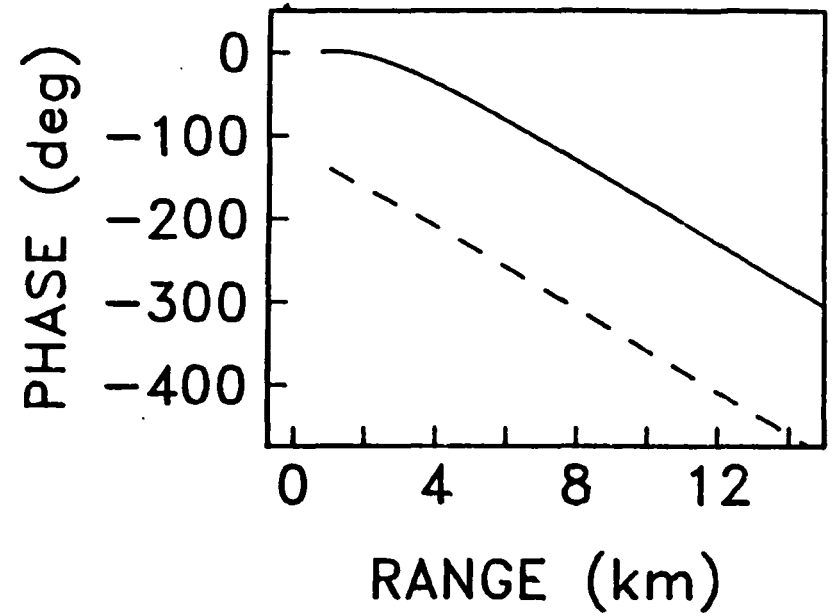
PHASE (deg)
0
−100
−200
−300
−400
0
4
8
12
RANGE (km)

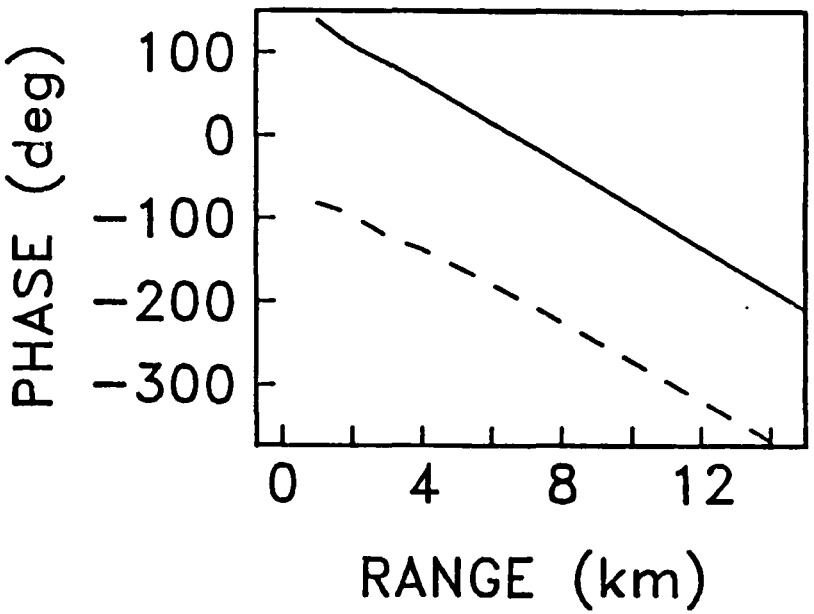
PHASE (deg)
100
0
−100
−200
−300
0
4
8
12
RANGE (km)

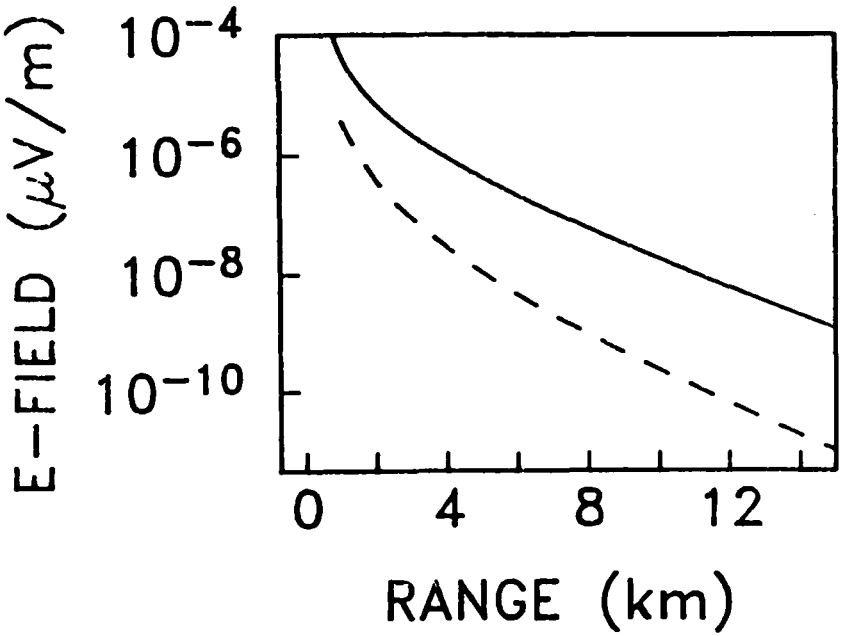
E−FIELD (μV/m)
10−4
10−6
10−8
10−10
0
4
8
12
RANGE (km)

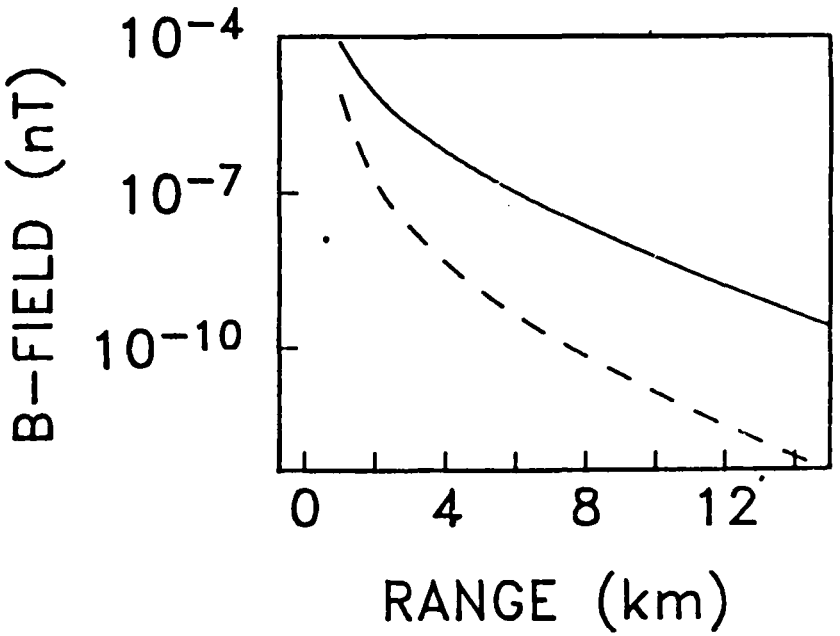
B−FIELD (nT)
10−4
10−7
10−10
0
4
8
12
RANGE (km)

Figure 2

The azimuthal magnetic field (top), radial electric field (bottom, solid line), and vertical electric field (bottom, dashed line) as a function of range at a frequency of 1 Hz produced by a borehole VED source and observed on the seafloor. The source is assumed to occupy the upper 500 m of the rock with a source moment of 1 A-m. The conductivity model is that of Figure 1.

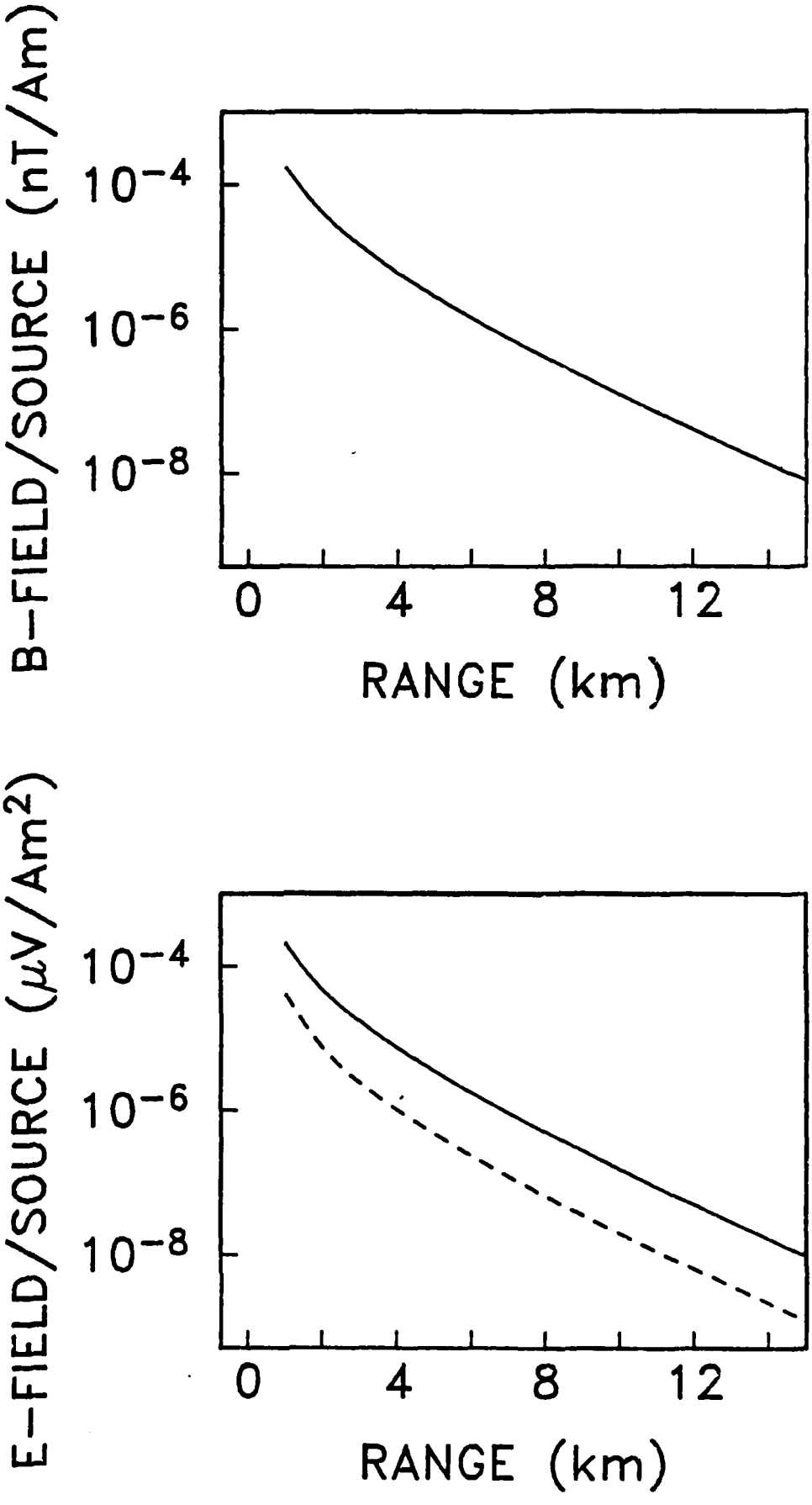
B-FIELD/SOURCE (nT/Am)
10^{-4}
10^{-6}
10^{-8}
0
4
8
12
RANGE (km)
E-FIELD/SOURCE (μV/Am^2)
10^{-4}
10^{-6}
10^{-8}
0
4
8
12
RANGE (km)

Fig 2

Figure 3

The electric and magnetic fields produced at 500 m depth in the rock halfspace of Figure 1 by a seafloor HED source. The top panel shows the radial (solid) and vertical (dashed) magnetic fields at an azimuth of 90^{o}, while the bottom panel shows the radial (solid) and vertical (dashed) electric fields. The remaining parameters are as for Figure 1.

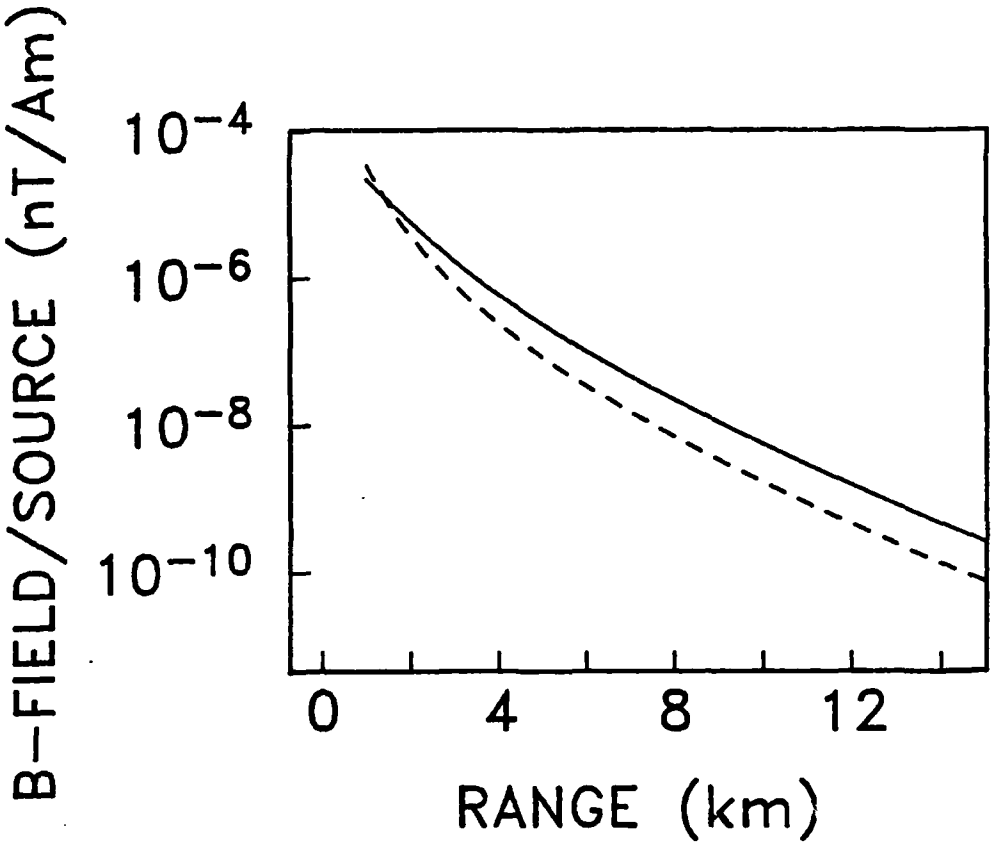
B-FIELD/SOURCE (nT/Am)
10^{-4}
10^{-6}
10^{-8}
10^{-10}
0
4
8
12
RANGE (km)

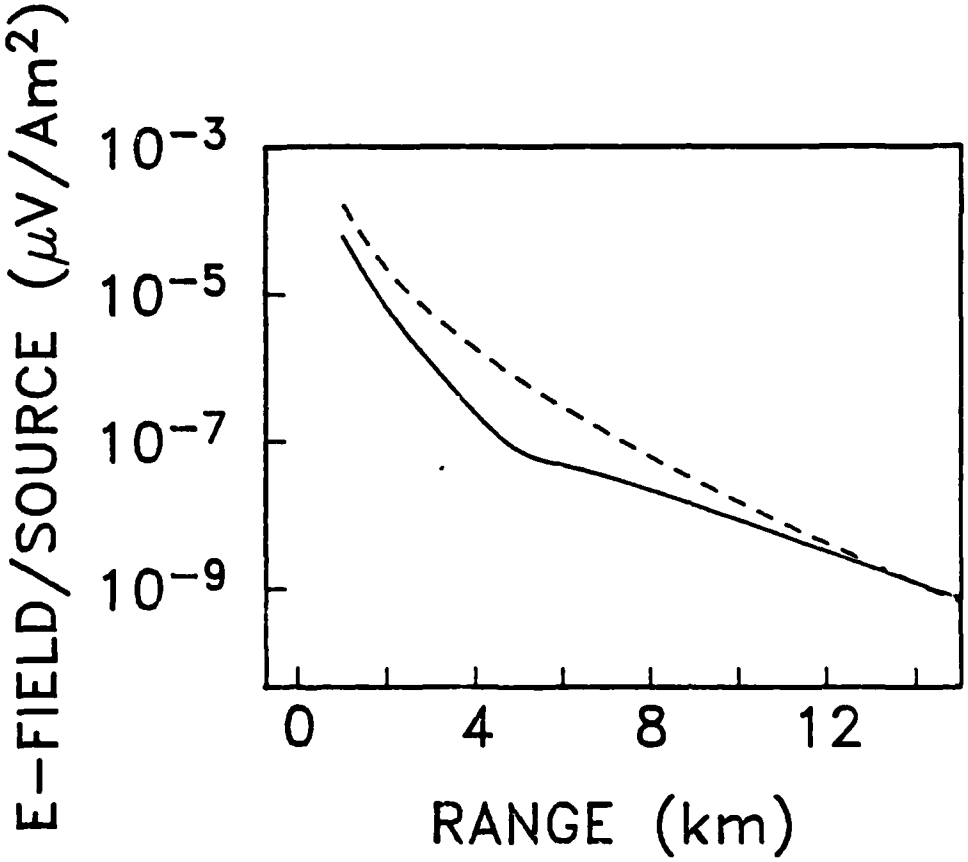
E-FIELD/SOURCE (μV/Am^2)
10^{-3}
10^{-5}
10^{-7}
10^{-9}
0
4
8
12
RANGE (km)

Fig 3

Figure 4

The radial electric field at an azimuth of 0^{o} for a mature oceanic crust model consisting of a 1 km, 0.05 S/m pillow and flow basalt layer, a 2.5 km, 0.003 S/m gabbro layer, and a 2 km, 0.001 S/m sheeted dike region overlying a 0.0005 S/m mantle halfspace. The left panels show the fields as a function of source frequency at ranges of 4 km (solid line), 10 km (short dashed line), and 16 km (long dashed line). The right panels show the fields at ranges of 3 km (short dashed line), 4 km (solid line), 5 km (long dashed line), and 8 km (dash-dot line). The field amplitudes are for a 1 A-m source strength. (Taken from Chave and Cox (1982), Figs. 10 and 11)

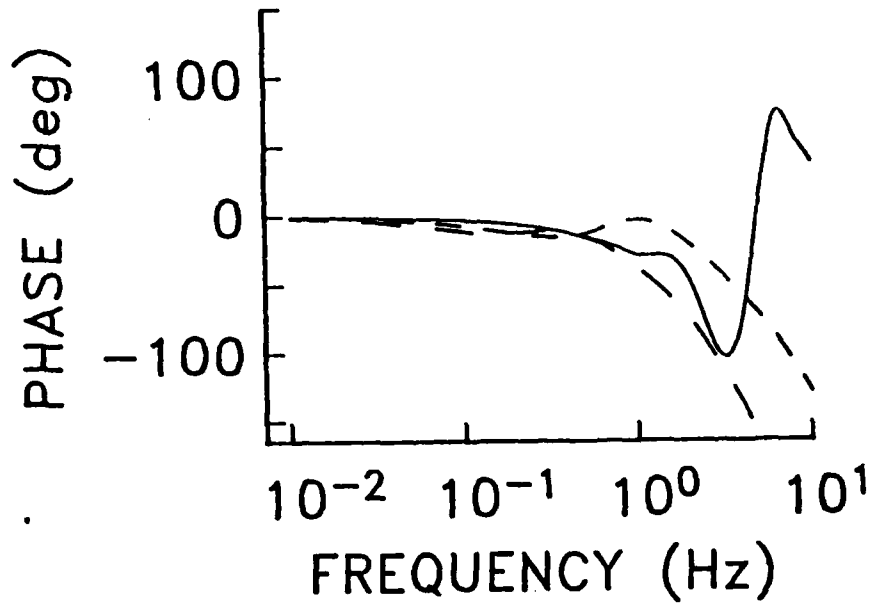
PHASE (deg)
100
0
−100
10^{-2} 10^{-1} 10^{0} 10^{1}
FREQUENCY (Hz)

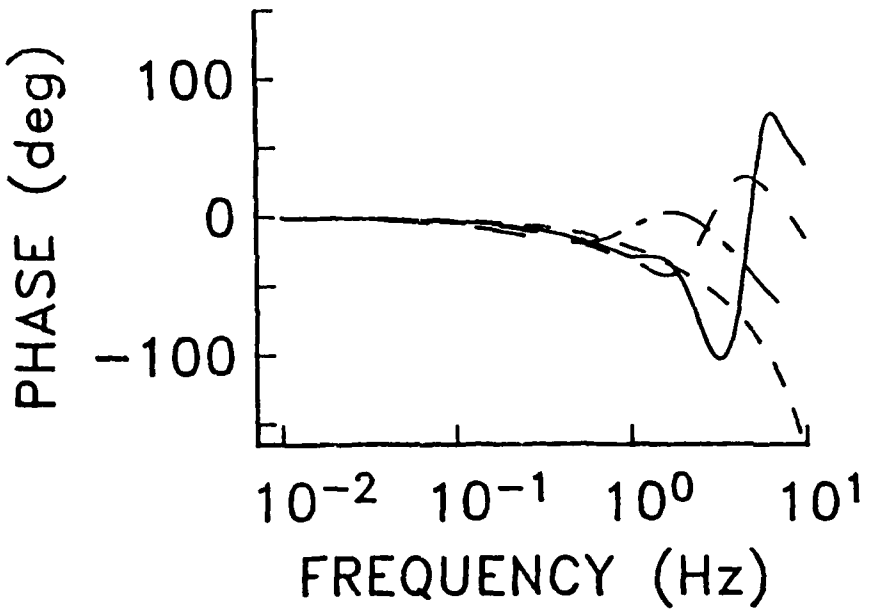
PHASE (deg)
100
0
−100
10^{-2} 10^{-1} 10^{0} 10^{1}
FREQUENCY (Hz)

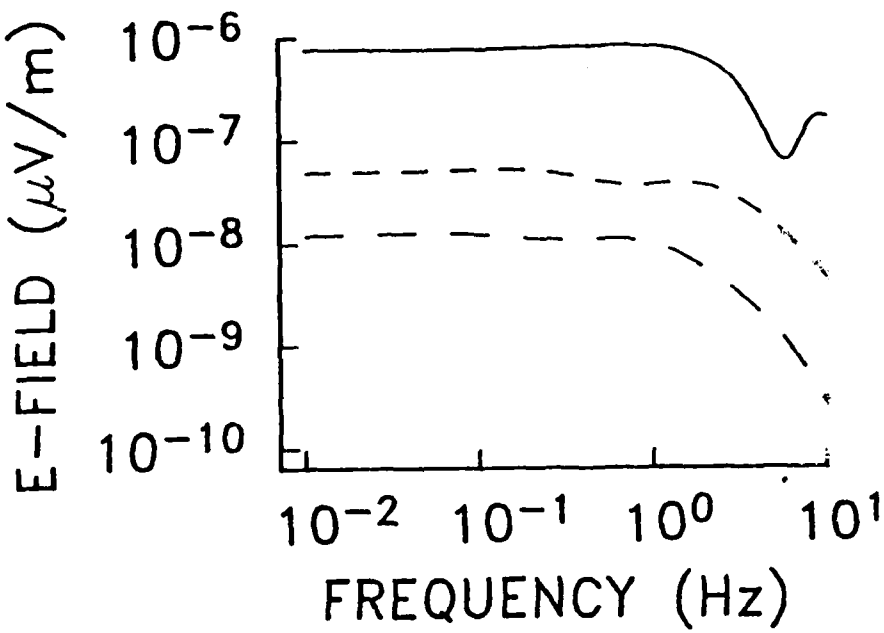
E-FIELD (μV/m)
10^{-6}
10^{-7}
10^{-8}
10^{-9}
10^{-10}
10^{-2} 10^{-1} 10^{0} 10^{1}
FREQUENCY (Hz)

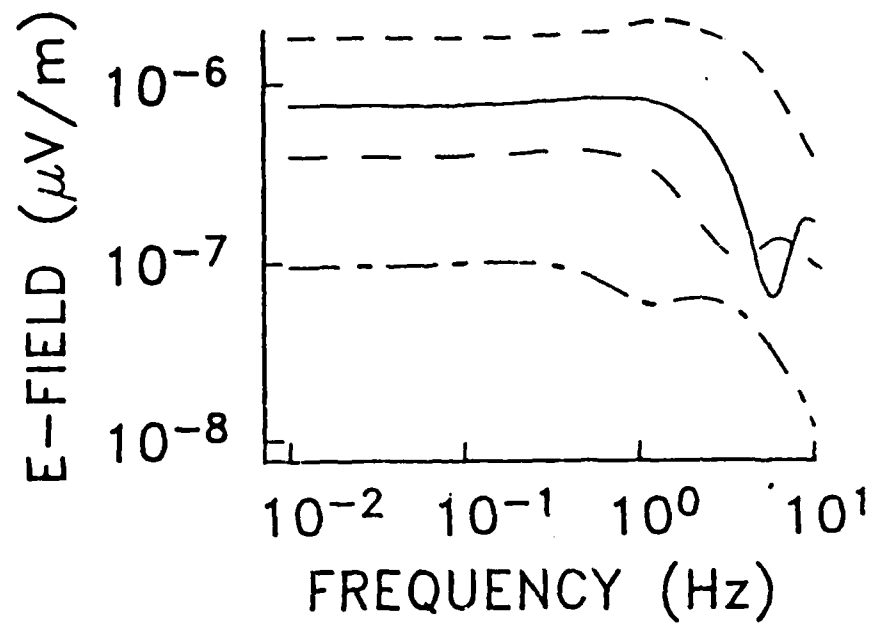
E-FIELD (μV/m)
10^{-6}
10^{-7}
10^{-8}
10^{-2} 10^{-1} 10^{0} 10^{1}
FREQUENCY (Hz)

Fig 4

Figure 5

The radial electric field produced at the seafloor by a borehole VED occupying the upper 500 m of the same model of Figure 4. The left panels show the field at ranges of 4 km (solid line), 10 km (short dashed line), and 16 km (long dashed line). The right panels show the field at ranges of 3 km (short dashed line), 4 km (solid line), 5 km (long dashed line), and 7 km (dash-dot line). The field amplitude is normalized to a source moment of 1 A-m, as for Figure 4.

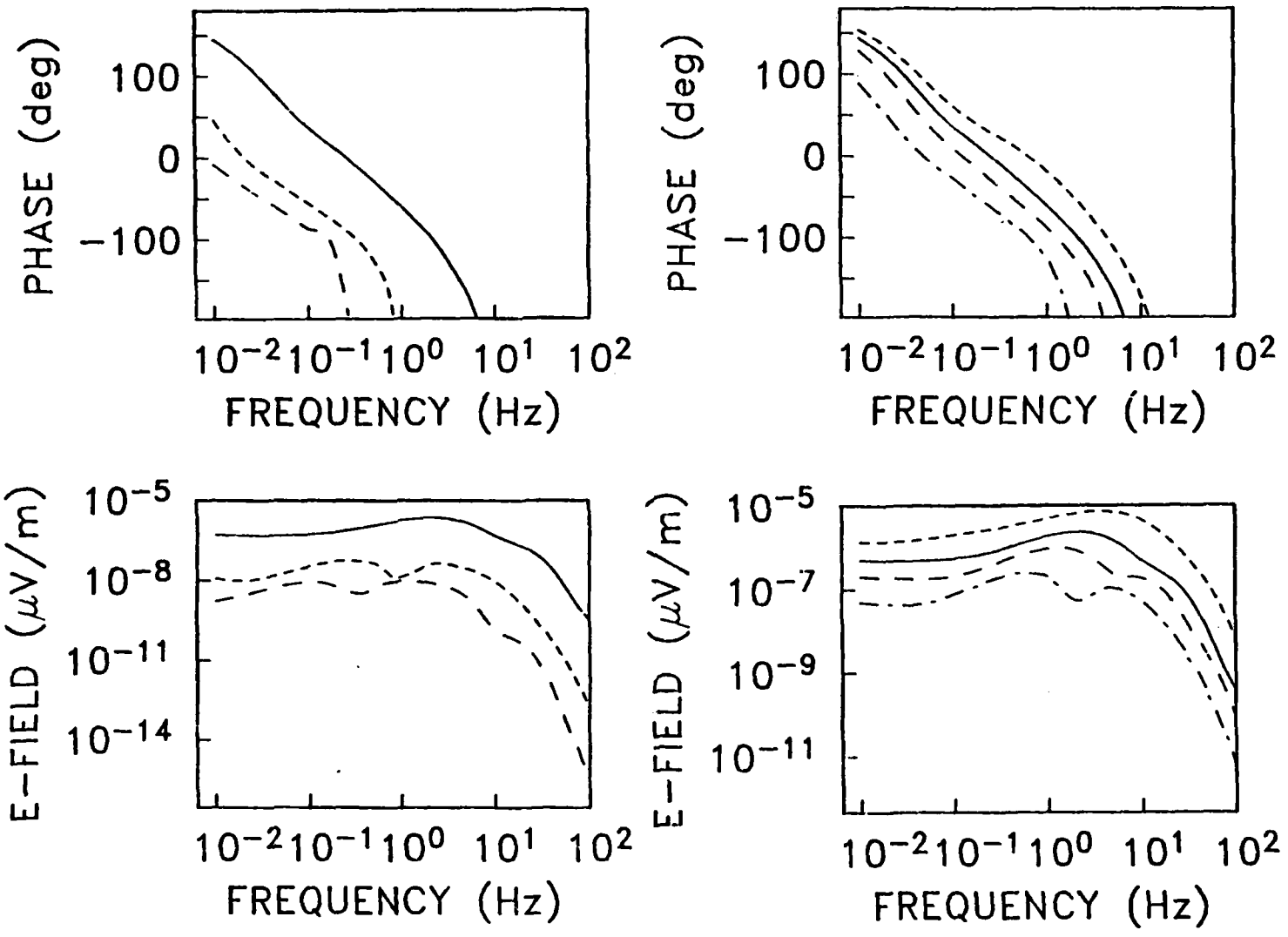
PHASE (deg)
100
0
−100
10^{-2} 10^{-1} 10^{0} 10^{1} 10^{2}
FREQUENCY (Hz)
PHASE (deg)
100
0
−100
10^{-2} 10^{-1} 10^{0} 10^{1} 10^{2}
FREQUENCY (Hz)
E-FIELD (μV/m)
10^{-5}
10^{-8}
10^{-11}
10^{-14}
10^{-2} 10^{-1} 10^{0} 10^{1} 10^{2}
FREQUENCY (Hz)
E-FIELD (μV/m)
10^{-5}
10^{-7}
10^{-9}
10^{-11}
10^{-2} 10^{-1} 10^{0} 10^{1} 10^{2}
FREQUENCY (Hz)

Figure 6

The azimuthal magnetic field at an azimuth of 0^{o} produced at the seafloor by a seafloor HED source for the same crustal model as in Figure 4. The left panels show the ranges 4 km (solid line), 10 km (short dashed line), and 16 km (long dashed line). The right panels show the ranges 3 km (short dashed line), 4 km (solid line), 5 km (long dashed line), and 7 km (dash-dot line). The field amplitude is normalized to a source moment of 1 A-m.

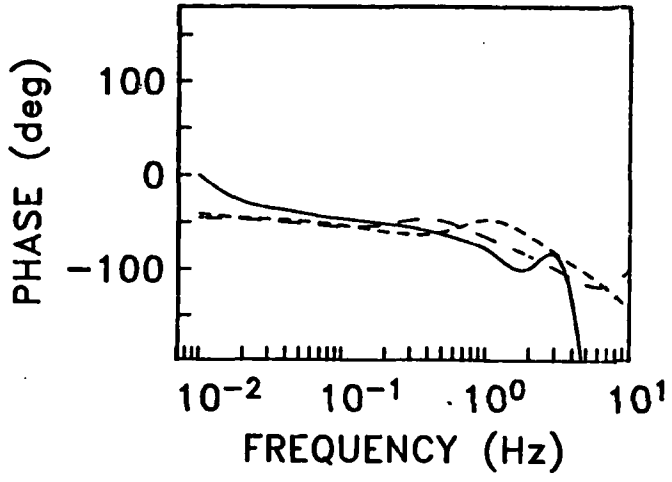
PHASE (deg)
100
0
−100
10^{-2}
10^{-1}
10^{0}
10^{1}
FREQUENCY (Hz)

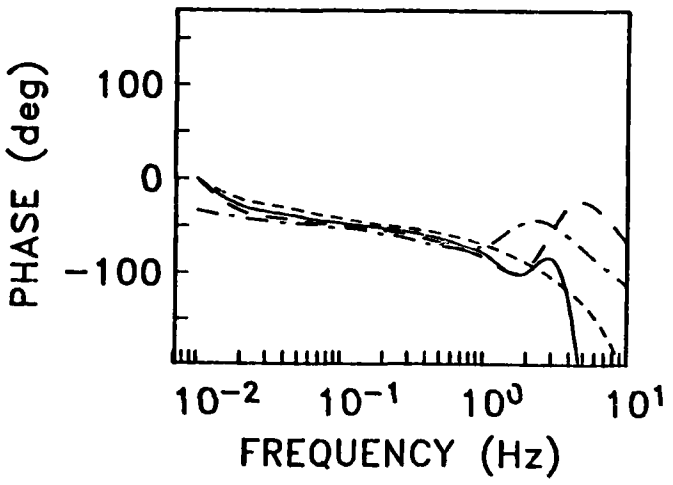
PHASE (deg)
100
0
−100
10^{-2}
10^{-1}
10^{0}
10^{1}
FREQUENCY (Hz)

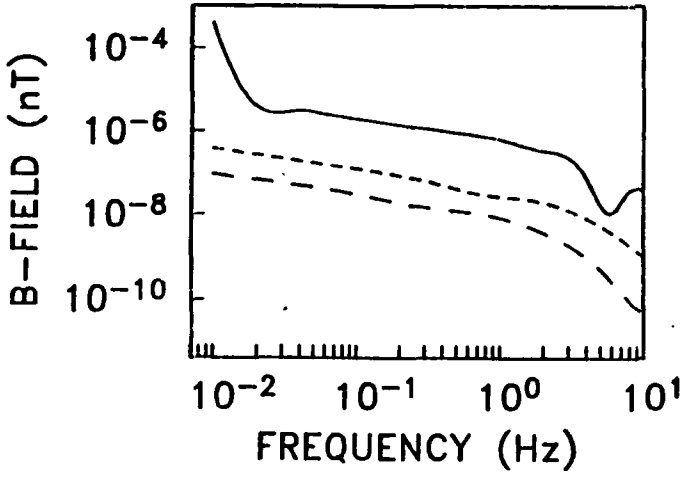
B-FIELD (nT)
10^{-4}
10^{-6}
10^{-8}
10^{-10}
10^{-2}
10^{-1}
10^{0}
10^{1}
FREQUENCY (Hz)

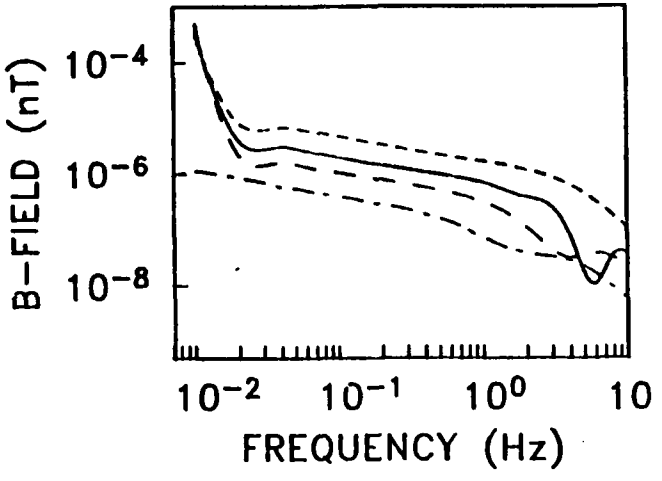
B-FIELD (nT)
10^{-4}
10^{-6}
10^{-8}
10^{-2}
10^{-1}
10^{0}
10
FREQUENCY (Hz)

Figure 7

The azimuthal magnetic field at an azimuth of 0° produced at a depth of 500 m in the upper layer of the crust by a seafloor HED. The remaining parameters are as in Figure 6.

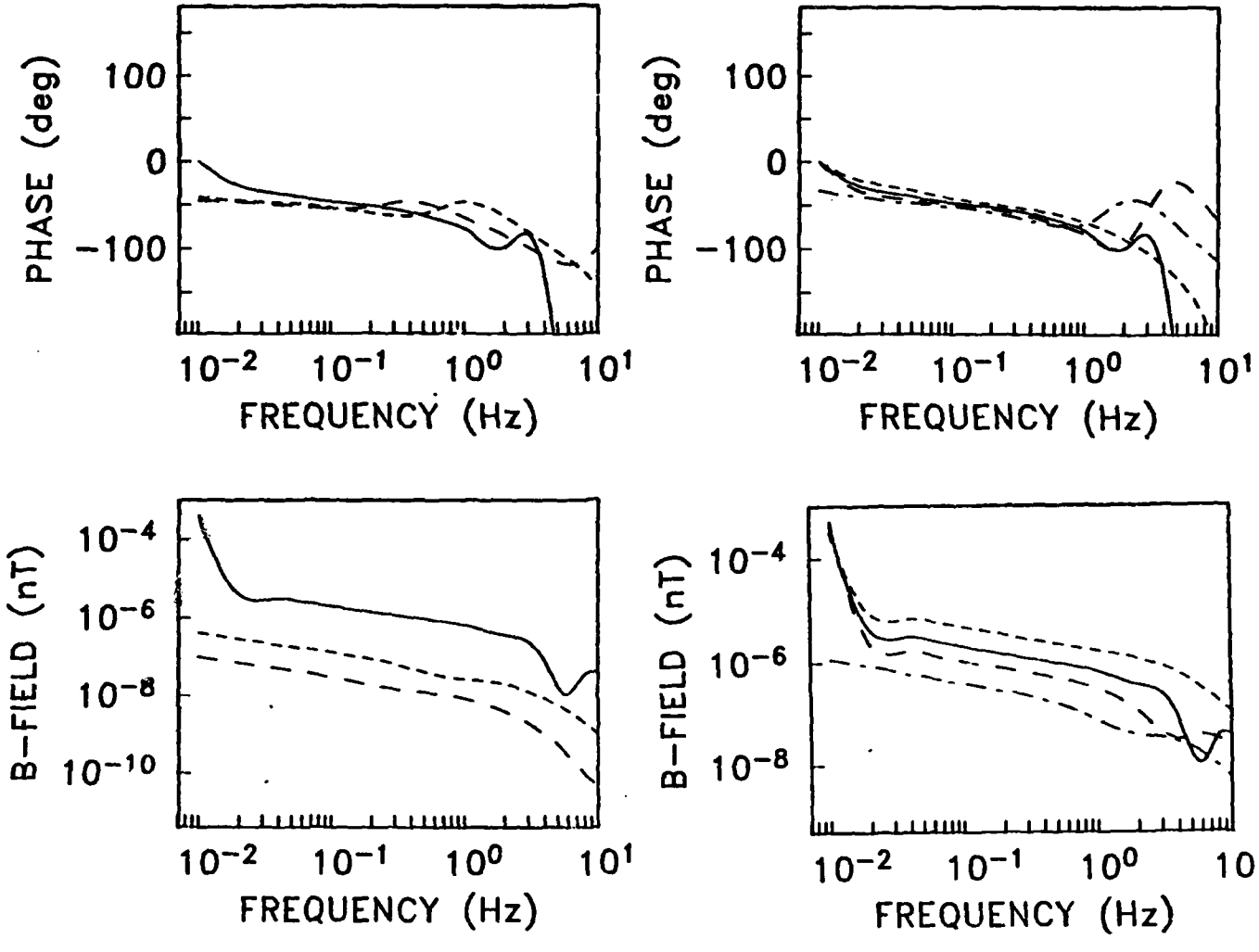
PHASE (deg)
100
0
−100
10^{-2} 10^{-1} 10^{0} 10^{1}
FREQUENCY (Hz)
PHASE (deg)
100
0
−100
10^{-2} 10^{-1} 10^{0} 10^{1}
FREQUENCY (Hz)
B-FIELD (nT)
10^{-4}
10^{-6}
10^{-8}
10^{-10}
10^{-2} 10^{-1} 10^{0} 10^{1}
FREQUENCY (Hz)
B-FIELD (nT)
10^{-4}
10^{-6}
10^{-8}
10^{-2} 10^{-1} 10^{0} 10
FREQUENCY (Hz)

Figure 8

Three models, numbered 1-3 from top to bottom, for an oceanic lithosphere containing a low conductivity channel. For the high and low conductivity borehole cases (see text), the upper 500 m of the lithosphere is replaced by a layer of conductivity 0.05 S/m and 0.005 S/m respectively.

Model 1

0.5	3.2
5	.003
4	.0002
10	10^{-6}
HS	10^{-5}

Model 2

0.5	3.2
5	.003
4	.0002
10	10^{-5}
HS	5×10^{-5}

Model 3

0.5	3.2
5	.003
4	5×10^{-5}
10	10^{-5}
HS	5×10^{-5}

Figure 9

The radial electric field at an azimuth of 0^{o} for Model 1. The ranges 30 km (top) and 70 km (bottom) are shown. The solid line represents the seafloor HED to seafloor case, while the borehole VED results in high (0.05 S/m) and low (0.005 S/m) conductivity crust are shown as long and short dashed lines, and the borehole HED result in high and low conductivity crust are shown as dash-dot and dash-dot-dot lines respectively. The field amplitude is normalized to a source moment of 1 A-m.

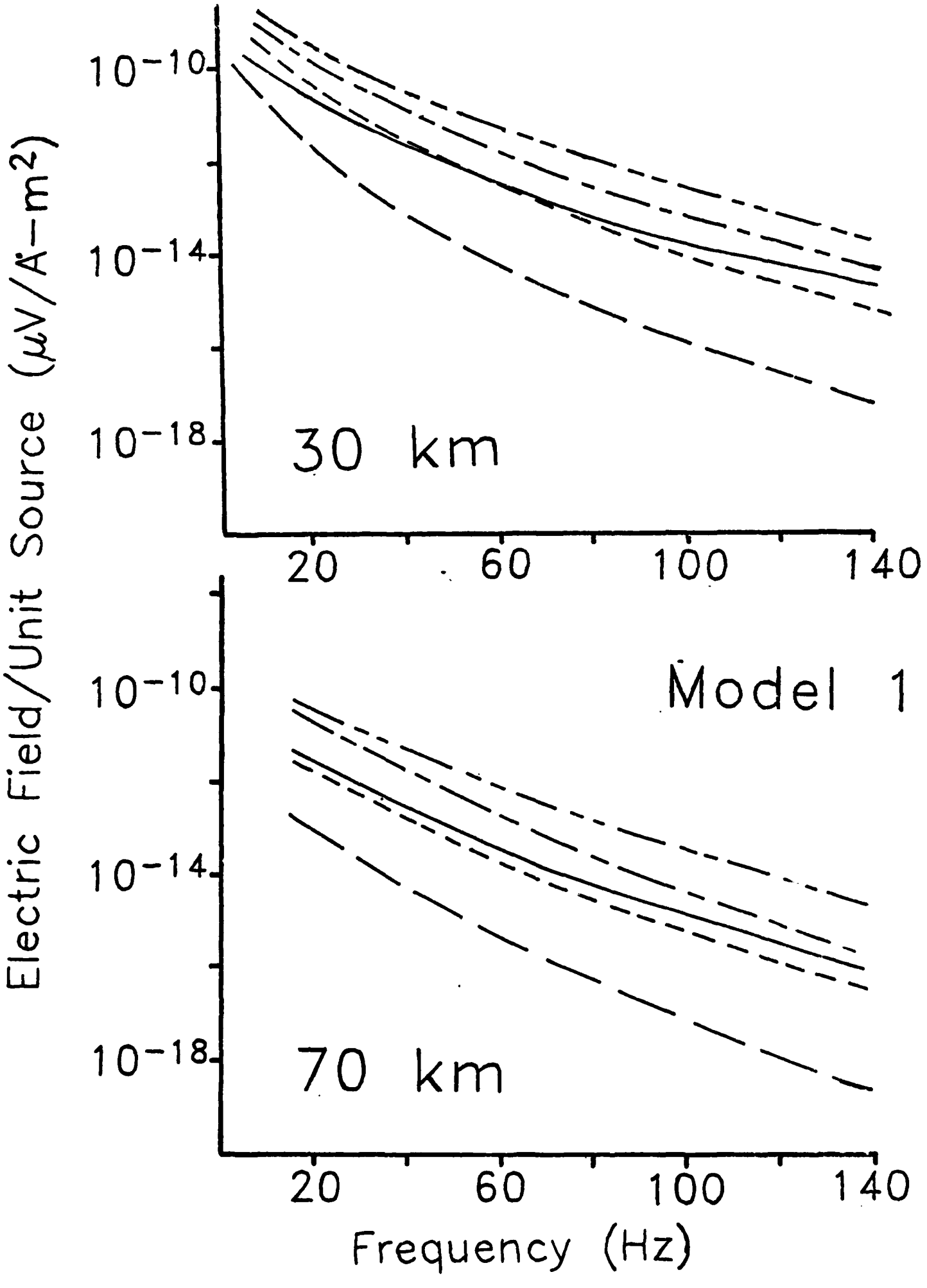
Electric Field/Unit Source (μV/A-m²)
10⁻¹⁰
10⁻¹⁴
10⁻¹⁸
30 km
20
60
100
140
Model 1
10⁻¹⁰
10⁻¹⁴
10⁻¹⁸
70 km
20
60
100
140
Frequency (Hz)

Figure 10

The radial electric field at an azimuth of 0^{o} for Model 2. See Figure 9 caption for details.

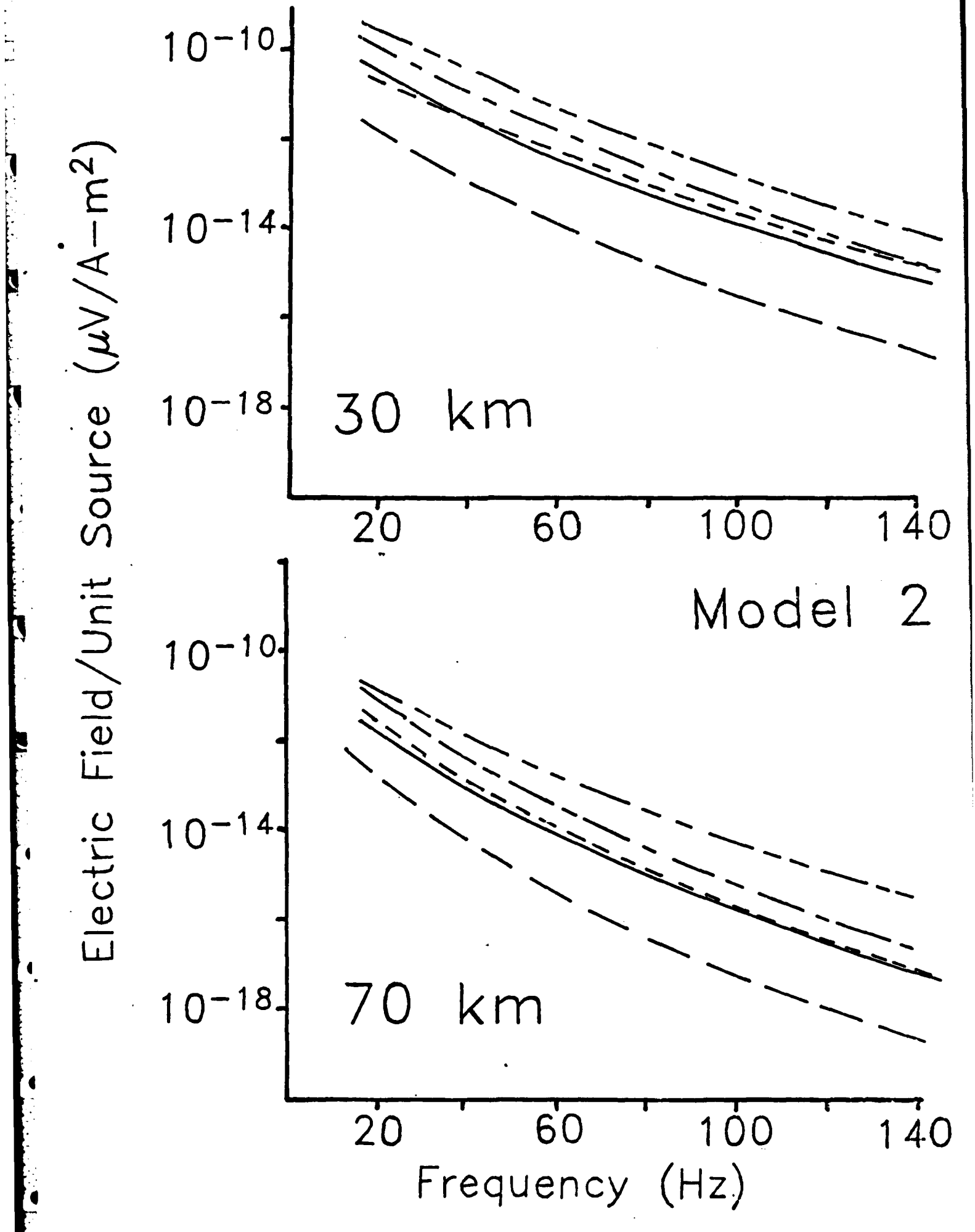
Model 2
30 km
70 km
10^{-10}
10^{-14}
10^{-18}
20
60
100
140
Electric Field/Unit Source ($\mu V/A-m^2$)
Frequency (Hz)

Figure 11

The radial electric field at an azimuth of 0^{o} for Model 3. See Figure 9 caption for details.

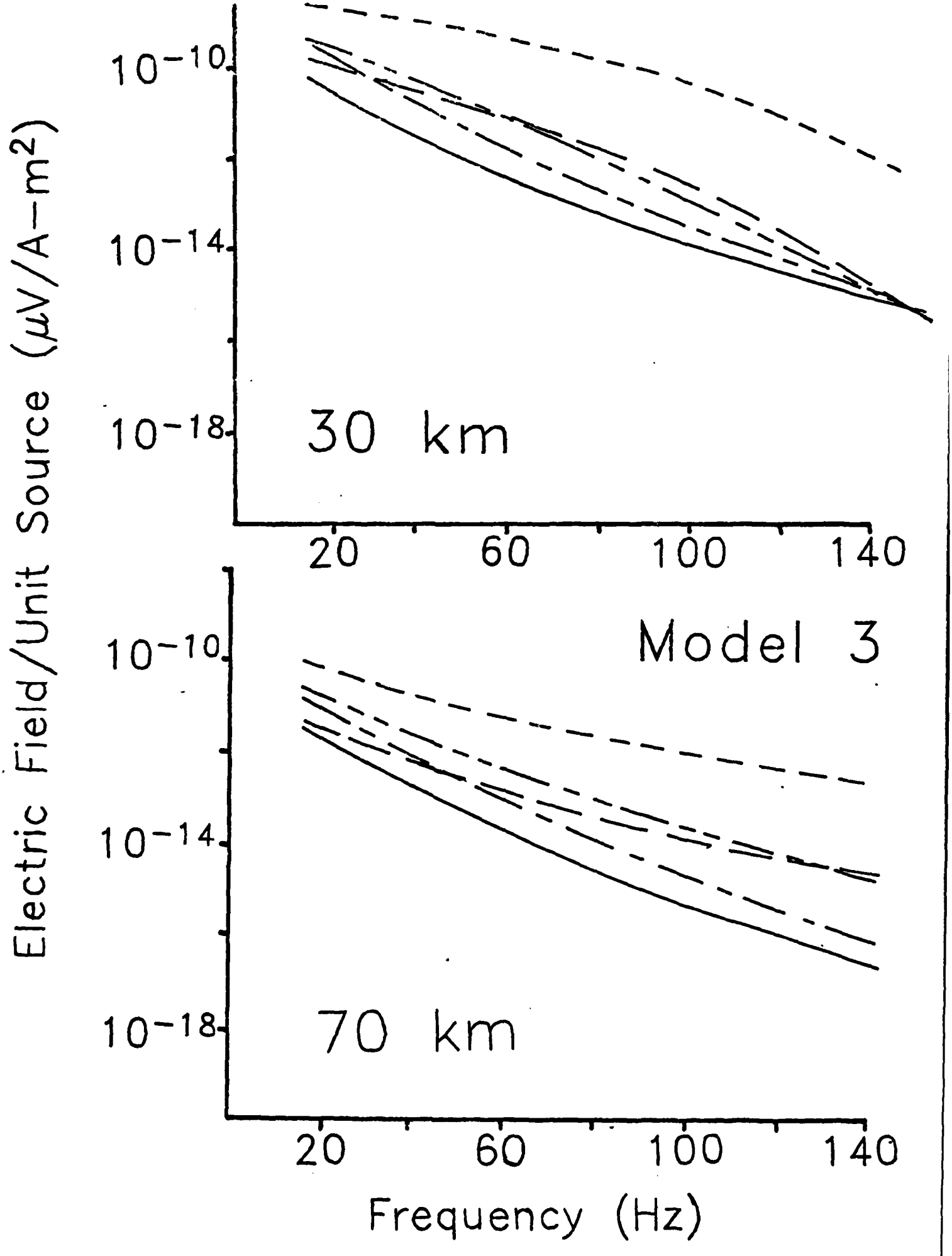
Electric Field/Unit Source ($\mu V/A-m^2$)
10^{-10}
10^{-14}
10^{-18}
30 km
20
60
100
140
Model 3
10^{-10}
10^{-14}
10^{-18}
70 km
20
60
100
140
Frequency (Hz)

MANADATORY DISTRIBUTION LIST

FOR UNCLASSIFIED TECHNICAL REPORTS, REPRINTS & FINAL REPORTS

PUBLISHED BY OCEANOGRAPHIC CONTRACTORS

OF THE OCEAN SCIENCE AND TECHNOLOGY DIVISION

OF THE OFFICE OF NAVAL RESEARCH

(Revised July 1978)

Department of Defense

Office of the Secretary of Defense (3)
Assistant Director of Defense Research
& Engineering
Washington, D.C. 20301

Navy

Office of Naval Research (3)
Code 460
Arlington, VA 22217

Office of Naval Research
Code 480
Arlington, VA 22217

Office of Naval Research
Code 102 B
Arlington, VA 22217

Office of Naval Research (6)
Code 102 DI
Arlington, VA 22217

Office of Naval Research
Commanding Officer
1030 East Green Street
Pasadena, CA 91101

Naval Ocean Research & Development
Activity
NORDA, Code 300
NSTL Station
Bay St. Louis, MS 39529

Naval Research Laboratory (6)
Library, Code 2620
Washington, D.C. 20375

U.S. Naval Oceanographic Office
Library, Code 8170
NSTL Station
Bay St. Louis, MS 39529

Other Government Agencies

Defense Documentation Center (12)
Cameron Station
Alexandria, VA 22314

National Oceanic & Atmospheric
Administration
National Oceanographic Data Center
Washington Navy Yard
Rockville, MD 20852